XXIst Moriond Astrophysics Meeting - Les Arcs March 10-17, 2001

THE TEMPERATURE PROFILE OF A1835 DETERMINED WITH XMM-NEWTON OBSERVATIONS AND THE IMPORTANCE OF ACCURATE BACKGROUND MEASUREMENTS

Sébastien Majerowicz & Doris M. Neumann
CEA/DSM/DAPNIA/SAp Saclay, 91191 Gif–sur–Yvette, France

We present a study of the galaxy cluster Abell 1835 observed with XMM-NEWTON. We focus on the determination of the temperature profile of the intra cluster medium (hereafter ICM). We find a temperature profile which is consistent with being constant or with showing a slight decrease at large radii (up to 1.2 Mpc). We observe a temperature drop in the center due to the cluster's cooling flow. The accurate knowledge of the background plays an important role in the temperature determination. We describe the different background components, astrophysical and instrumental, and a proper way how to correct for them.

1 Introduction

Using the hydrostatic equation to determine the mass profile of clusters of galaxies requires the precise knowledge of the temperature distribution of the hot X–ray emitting ICM. Due to the limitations in resolution and sensitivity of past X–ray observatories determining the temperature distribution was very difficult. Today, the next generation of X–ray satellites like XMM–NEWTON[6] and Chandra[12] allows us to overcome these difficulties and to constrain the temperature profile of clusters with unprecedented accuracy.

We present a study of the temperature profile of the medium distant (z$\sim$0.25) cluster Abell 1835, which was observed during the PV phase of XMM–NEWTON (see also Peterson[9]).

Clusters are extended X–ray sources with low surface brightness and consequently low signal-to-noise ratio far from its center. In order to determine the temperature in these regions accurately, one needs the precise knowledge on the different background components which are astrophysical as well as instrumental. Since the properties of the different background components vary across the field-of-view (FOV), we cannot apply a simple background subtraction method but have to develop a method for each component individually.

Due to instrument setting problems we concentrate solely on EPIC–MOS2 data. The PN data analysis is presented by T.Reiprich[10].

2 Flare rejection on EPIC–MOS cameras

The dynamical processes on galaxy cluster scales occur on time scales in order of 10^9 years. Therefore, we can assume the cluster X–ray emission coming from the ICM to be constant during an observation. However, we can see in figure 1 large variations of intensity in the light curve during the exposure. These variations are not caused by individual sources which lie in the FOV like for example AGN's. These intervals of high intensity are caused by particles which can be

observed in the entire FOV. From now on, these periods of high intensity will be called " flares ". It seems that they are correlated with solar eruptions and are mainly composed by soft energy protons which show variations in their energy spectrum. In order to enhance the signal-to-noise ratio, we discard these time intervals of high particle flux.

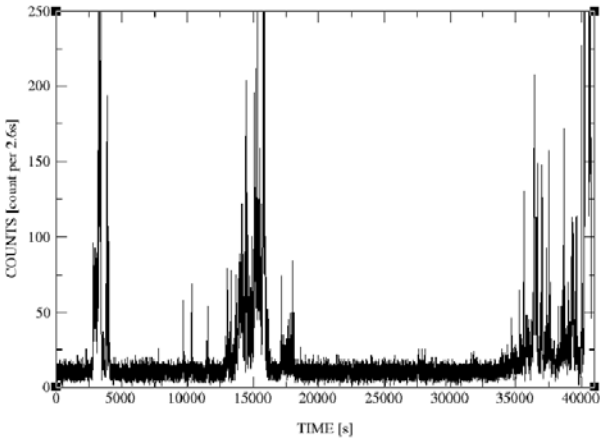

Figure 1: Abell 1835 light curve for event energy from 0.3 to 12 keV.

The MOS cameras have very low sensitivity for X–ray photons above 10 keV. Furthermore the soft energy protons which are responsible for the observed flares show a hard energy tail in the spectrum can be detected above 10 keV in the MOS cameras. Therefore, the spectral band above 10 keV is ideally suited to monitor flares. We choose the energy band 10 to 12 keV as a tracer for flare periods. To trace intervals dominated by high particle flux we bin the light curve in bins of 100 seconds in order to have sufficient statistics. We reject all bins above a certain threshold. The relationship between this threshold and the remaining exposure time is displayed in the figure 2. In the following analysis we adopt a threshold of 15 events per 100 sec bin in the 10 to 12 keV energy band which seems to be good compromise between time intervals without flares and remaining exposure time.

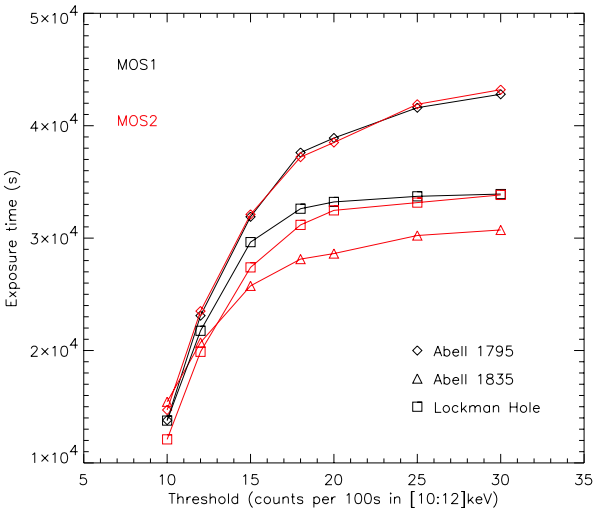

Figure 2: Exposure time versus count threshold for several data set.

The selection of the energy band allows us to apply the same threshold criterion not only

for the source observation but also for bank–field observations which can be used as background observations. To demonstrate the flare selection efficiency to enhance the signal-to-noise, we show in figure 3 the 0.5–5 keV images of Abell 1835 before and after flare rejection.

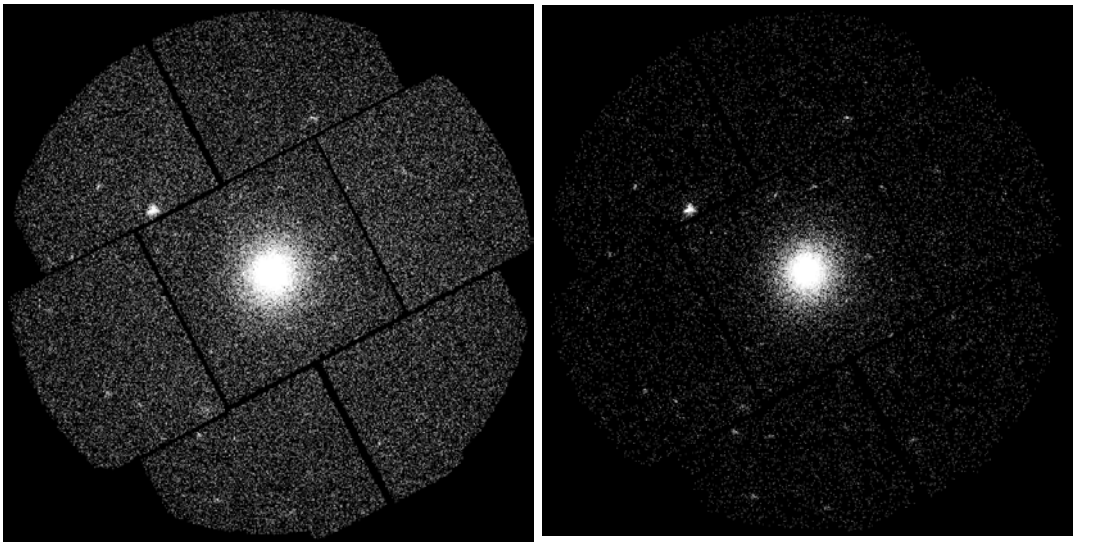

(a) (b)

Figure 3: Vignetted 0.5–5 keV images of Abell 1835 before (a) and after (b) our flare rejection method.

3 Vignetting correction

The sensitivity of the X–ray telescopes aboard XMM–NEWTON is not constant across the FOV but decreases with increasing off–axis angle. This decrease is also energy dependent and is generally called vignetting. To correct for this effect we adopt the photon weighting method which was developed at CEA–Saclay. The method[2] consists in calculating a weight parameter for each event, which is defined as the ratio of on–axis sensitivity versus sensitivity at the event position on the detector. In using these weight factors for each event we automatically correct for vignetting.

4 Background correction and its effect on the Abell 1835 temperature profile

To determine the background, we use different blank–field observations :

- the revolution 71 of the Lockman Hole (hereafter LH) ;
- the compilation of removed point source observations kindly provided by David Lumb (hereafter DL).

Figure 4 shows the spectra extracted from a 7' to 12' annulus around the cluster. The spectra take into account the vignetting via the photon weighting method (see above). The spectra consist of several components :

- the cosmic X–ray background (hereafter CXB) which is made up by photons and is consequently vignetted. This background component dominates at low energy ;

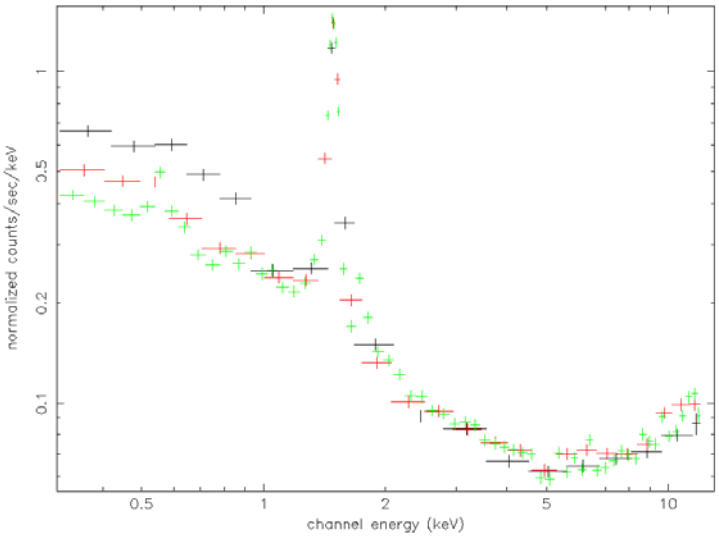

Figure 4: Vignetting corrected background spectra : Lockman Hole (rev. 71), David Lumb's blank–fields and the outer regions of Abell 1835 observation.

- high energy particles like cosmic–rays pass through the satellite and depose a fraction of their energy on the detector. They are not affected by the telescope vignetting. Since we corrected the spectra with the photon weight, which accounts for the falsely attributed vignetting, we see an artificial increase in the spectra at high energy. The weight factors are largest at high energies since the vignetting effect increases with energy [4] ;

- instrumental lines like the Aluminium feature around 1.4 keV which come from fluorescence of camera materials, which are excited from particles with high energies.

We can remark that above 2 keV all 3 spectra are dominated by the high energy particle component. The spectra in this energy range resemble each other. Below 1 keV the spectra are all different since the CXB varies considerably across the sky[11]. In order to correct for the different background components one needs to develop a background subtraction method, which takes into account the nature of the different backgrounds.

A straight forward solution to subtract for the instrumental and particle background is to subtract the background from a blank–field observation at the same detector position as the source with an appropriate normalization. This normalization is determined by the ratio of the flux above 10 keV between source and background observation. The normalization varies typically between 0.9 and 1.1.

The CXB varies across the sky and is therefore not necessarily the same between source and blank–field observation. Therefore, the blank–field observation is not a good representation of the CXB at the source position. In order to constrain the CXB at the source position we use the outer regions (7'<r<12') of the Abell 1835 observation. We subtract the blank–field observation in the same region in order to correct for the particle background. The remaining residuals are exclusively coming from the differences between CXB around the source position and the blank-sky observation. Re–subtracting these residuals from the previously obtained spectrum of Abell 1835 provides an accurate subtraction of all the different background components.

Finally, we fit the background subtracted spectra, which we binned into 3 sigma bins, with a Mekal code[8] with a galactic absorption of $n_H = 2.24 \times 10^{20}$ cm^{-2}. The best fit results (90% confidence level) are shown in figure 5. (a) shows the temperature profile and (b) the corresponding abundance profile.

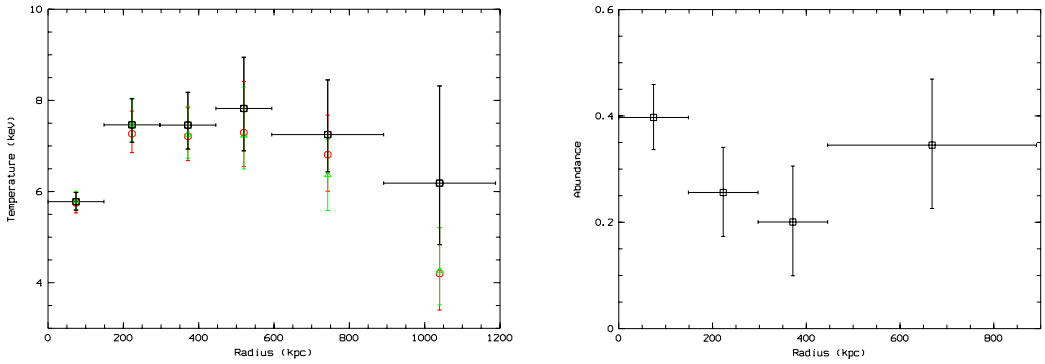

(a) Temperature (b) Abundance

Figure 5: Abell 1835 profiles (same color convention than for the figure 4).

5 Discussion

5.1 Data treatment

XMM–NEWTON observations often suffer from time intervals with high particle flux which introduce an important background component. To enhance the signal-to-noise ratio we reject these high flux periods.

In order to correct for the remaining different background components, astrophysical and instrumental or better high energy particle background we perform a double background subtraction. This correction must be done correctly to avoid a bias in the temperature estimate. Indeed, if we do not correct for the high energy particle background which has a hard spectrum, our temperature estimate will be too high. If we neglect the local CXB, which is relatively high at the position of Abell 1835, we underestimate the temperature since the CXB has a soft spectrum (see figure 5 (a) where there is a difference of 2 keV for the derived temperature in the last annulus).

5.2 The remaining profiles

We determine a temperature profile of Abell 1835 up to 1.2 Mpc which corresponds roughly to 0.5 times the virial radius[5] (hereafter r_V) and an element abundance profile up to r/r_V=0.4 . r_V is calculated assuming a constant temperature of 7.5 keV and fixed redshift at z=0.25.

The temperature profile (see figure 5 (a)) of Abell 1835 falls off towards the center due to the cooling flow and shows a light tendency to decrease with increasing radius. However, we cannot exclude that the cluster is isothermal outside the cooling flow region. This flatness outside the region of true cooling flow is in agreement with the other recent measured temperature profiles[3] from clusters observed by XMM–NEWTON. Figure 6 shows our temperature profile of Abell 1835 as compared to a recently suggested universal kT profile[7] from a compilation of ASCA temperature profiles. It seems that this cluster does not follow this type of profile. However Abell 1835 is a medium redshift cluster and maybe cannot be directly compared with the sample of Markevitch[7] which was based only on nearby clusters. Nevertheless our temperature profile is in agreement with the sample of White[13] (clusters within 0.003<z<0.55) where 90% of his clusters are consistent with isothermality. The temperature of $9.8\pm^{2.3}_{1.3}$ keV derived from ASCA[1] is significantly higher than our temperature estimate. However, this temperature estimate was calculated with a multi–phase cooling flow model which might bias the measured ambient ICM

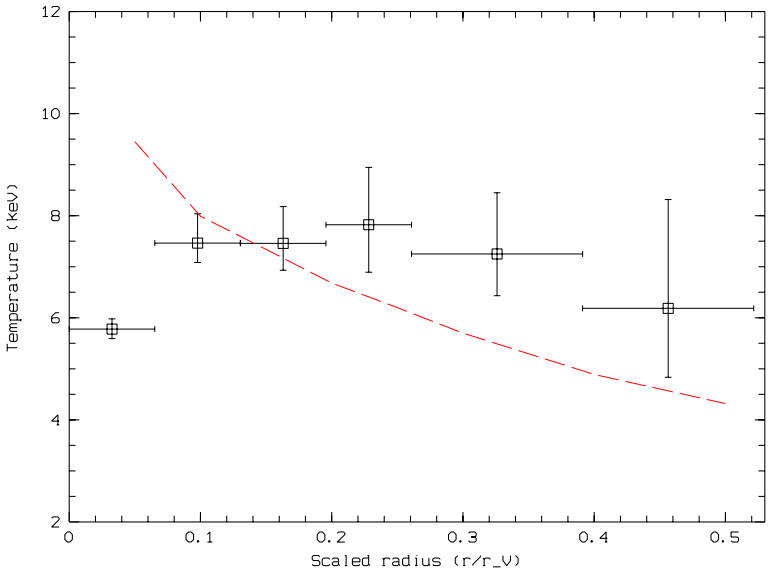

Figure 6: Radial temperature profile of Abell 1835 with our best background subtraction. The dashed red line is the temperature profile obtained by Markevitch et al. 1998 normalized to the virial radius and the mean temperature of Abell 1835.

temperature.

Concerning the iron abundance profile (see figure 5 (b)), no conclusions about a variation with increasing radius could be drawn but we can exclude great variations outside the cooling flow.

6 Conclusion

In this paper we present the different background components of XMM–NEWTON observations. We present a coherent approach to correct for each background component such as flares, high energy particles and astrophysical background. We show that background subtraction is extremely important in regions with low surface brightness where the signal-to-background ratio is very low.

We show that the temperature profile is consistent with an isothermal ICM outside the cooling flow area but shows a slight tendency to decline with radius.

For this study we only used one EPIC–MOS camera. To obtain more stringent conclusions concerning the temperature profile, it is necessary to combine all EPIC cameras aboard XMM–NEWTON.

Acknowledgements

We would like to thank M. Arnaud for useful discussions, the whole team in CEA–Saclay for developing software and Thomas Reiprich at MPE with whom we had useful discussions concerning data treatment and results.

1. Allen S.W., Fabian A.C., MNRAS **297**, L57 (1998)
2. Arnaud M., Neumann D.M., Aghanim N., Gastaud R., Majerowicz S., Hughes J.P., A&A **365**, L80 (2001)
3. Arnaud M., *these proceedings*
4. Dahlem M., XMM–NEWTON User's Handbook, http://xmm.vilspa.esa.es/user/uhb/xmm_uhb.html

5. Evrard A.E., Metzler C.A., Navarro J.F., ApJ **469**, 494 (1996)
6. Jansen F., Lumb D., Altieri B., Clavel J., Ehle M., Erd C., Gabriel C., Guainazzi M., Gondoin P., Much R., Munoz R., Santos M., Schartel N., Texier D., Vacanti G., A&A **365**, L1 (2001)
7. Markevitch M., Forman W.R., Sarazin C.L., Vikhlinin A., ApJ **503**, 77 (1998)
8. Mewe R., Gronenschild E.H.B.M. & van den Oord G.H.J., A&AS **62**, 197 (1985)
9. Peterson J.R., Paerels F.B.S., Kaastra J.S., Arnaud M., Reiprich T.H., Fabian A.C., Mushotzky R.F., Jernigan J.G., Sakelliou I., A&A **365**, L104 (2001)
10. Reiprich T.H., *these proceedings*
11. Snowden S.L., Egger R., Freyberg M.J., McCammon D., Plucinsky P.P., Sanders W.T., Schmitt J.H.M.M., Trümper J., Voges W., ApJ **485**, 125 (1997)
12. Weisshopf M.C., Tananbaum H.D., Van Speybroeck L.P., O'Dell S.L., SPIE **4012**, 2 (2000).
13. White D.A., MNRAS **312**, 663 (2000)